Front. Chem. Sci. Eng. 2022, 16(4): 475–483
https://doi.org/10.1007/s11705-021-2070-x

RESEARCH ARTICLE

Non-thermal plasma enhances performances of biochar in wastewater treatment and energy storage applications

Rusen Zhou[1,2,3*], Xiaoxiang Wang[2,4*], Renwu Zhou[3], Janith Weerasinghe[2], Tianqi Zhang[3], Yanbin Xin (✉)[1], Hao Wang[4], Patrick Cullen[3], Hongxia Wang[2], Kostya (Ken) Ostrikov[2]

1 College of Environmental Science and Engineering, Dalian Maritime University, Dalian 116026, China
2 School of Chemistry and Physics and QUT Centre for Materials Science, Queensland University of Technology, QLD 4000, Australia
3 School of Chemical and Biomolecular Engineering, The University of Sydney, NSW 2006, Australia
4 Centre for Future Materials, University of Southern Queensland, QLD 4350, Australia

Abstract Surface functionalization or modification to introduce more oxygen-containing functional groups to biochar is an effective strategy for tuning the physicochemical properties and promoting follow-up applications. In this study, non-thermal plasma was applied for biochar surface carving before being used in contaminant removal and energy storage applications. The results showed that even a low dose of plasma exposure could introduce a high number density of oxygen-functional groups and enhance the hydrophilicity and metal affinity of the pristine biochar. The plasma-treated biochar enabled a faster metal-adsorption rate and a 40% higher maximum adsorption capacity of heavy metal ion Pb^{2+}. Moreover, to add more functionality to biochar surface, biochar with and without plasma pre-treatment was activated by KOH at a temperature of 800 °C. Using the same amount of KOH, the plasma treatment resulted in an activated carbon product with the larger BET surface area and pore volume. The performance of the treated activated carbon as a supercapacitor electrode was also substantially improved by $> 30\%$. This study may provide guidelines for enhancing the surface functionality and application performances of biochar using non-thermal-based techniques.

Keywords non-thermal plasma, surface functionalization, biochar modification, wastewater treatment, supercapacitor

Received February 24, 2021; accepted May 2, 2021

E-mail: xinyb33@dlmu.edu.cn

*These authors contributed equally to this work.

1 Introduction

Biomass, the only renewable but widely available organic carbon resource, offers an ideal clean alternative for fossil fuels to meet the soaring energy requirement due to the explosive population growth and rapid industrialization [1–3]. Using different valorization methods such as liquefaction, gasification, pyrolysis and microbial engineering, carbon-based biomass-derived fuels (gas, liquid and solid) and chemicals can be obtained [1,2,4]. Biochar is a solid bio-derived product produced by slow pyrolysis of biomass with limited or no O_2 supplied at a moderate temperature (usually lower than 700 °C) [1,5]. Due to its carbon-richness and renewability property, low-cost and high modifiability, biochar is widely used especially for environmental protection purposes and is well accepted as an ideal platform for developing many other functionalized carbon materials for further catalytic and energy- and environment-associated applications [1,5,6].

Generally, it is difficult to obtain a high efficiency of the pristine biochar in practical applications because of the poor surface functionality and the under-developed pore structure [5–7]. Thus, further processing, modification or functionalization of biochar, after being obtained from pyrolysis, for tuning surface properties and tailoring pore structure prior to its use is generally a prerequisite for performance enhancement [7,8]. Introducing different functional groups on the surface of biochar has been extensively studied using surface oxidation, amination, or sulphonation to provide high-density active sites effectively. Thus, the modified biochar can be used as a catalyst, catalyst support, or pollutant adsorbent [1]. The modification, however, generally requires the use of substantial fossil fuels-based chemicals and following procedures for residual chemical removal [7–9]. In addition, it is

worthwhile to note that to be used as an energy storage material, upgrading or tailoring the porosity and surface area of biochar is essential to achieve the enhanced mass transfer fluxes and active loading. It is usually targeted *via* further activation by physical heating and the addition of specific chemical reagents ($ZnCl_2$, H_3PO_4, KOH) as activators. The activation process is energy-intensive, and again, the use of an adequate amount of chemicals is warranted to obtain targeted properties [1,6,10].

It is commonly expected that introducing reactive chemical and physical effects for material functionalization may significantly improve the performance of specific applications. Plasmas, especially those non-thermal or low-temperature discharges, are effective for material processing because of the highly non-equilibrium characteristics of plasma with the coexistence of high energy electrons and high-density reactive species at low gas temperature as well as energetic photons, which enable the plasma-based treatments to be performed under mild conditions [4,11]. Moreover, plasmas also have other advantages, such as simple equipment types and, more importantly, chemical-free processing [12–15]. The efficacy of plasma treatment has been demonstrated in many surface treatment applications such as oxidation, modification and functionalization of polymers, metal catalysts and carbon materials, including activated carbons [16–18]. Herein, an air dielectric barrier discharge (DBD) plasma was used to process the biochar obtained by pyrolysis of bamboo shoot shell at 400 °C before it was applied as an adsorbent for the removal of heavy metal ion in wastewater and further activated by KOH at 800 °C. With the same amount of KOH, plasma pre-treatment resulted in an activated carbon product with higher porosity and increased specific surface area, which also showed better performances towards supercapacitors. Results indicated that plasma processing was effective in enhancing the surface functionality of biochar and reducing the use of chemical reagents in the activation process, making the biochar-based applications more economical and environmentally friendly.

2 Experimental

The schematic diagram on the experimental procedures is shown in Fig. 1, which mainly contains biochar preparation, plasma processing, activation, characterization, and applications. The specific process is as follows.

2.1 Biochar preparation

The bamboo shoot shell (BSS) was water-washed and oven-dried after being collected from the Brisbane City Botanic Gardens, Australia. The BSS was then crushed by a grinder and sieved to obtain 40-mesh BSS particles for further pyrolysis. Specifically, 30 g of BSS particles was placed in a quartz boat and then positioned at the middle of quartz tubular furnace under N_2 atmosphere (0.5 $L \cdot min^{-1}$) with a heating rate of 5 $°C \cdot min^{-1}$ starting from room temperature to set temperature of 400 °C (sustained at this temperature for 30 min) [19]. After the heating, the biochar obtained was left inside the furnace for natural cooling and termed as BSS-derived biochar (BSSBC).

2.2 Plasma processing

As-prepared BSSBC was placed in a reactor (DBD-100, Nanjing Suman, China) before introducing the discharge. The distance between the two steel electrodes connected to the power source (CTP-2000K, Nanjing Suman, China) and the ground was at ~10 mm. The peak-peak applied voltage was set at 30 kV, with the frequency fixed at 9 kHz. The ambient air was directly used as the working gas for the discharge. BSSBC was treated using air DBD discharge at atmospheric pressure with different treatment times (0, 0.5, 1.0, 5.0, 10, 20 and 30 min), and the sample obtained was assigned as BSSBC-P-X, where X represented the plasma exposure time.

2.3 Biochar activation

To obtain carbon materials with ideal performances for further energy- or catalysis-based applications from biochar, activation is necessary. Here, both pristine BSSBC and plasma-treated BSSBC were subjected to a commonly used activation process (activation by potassium hydroxide). The biochar samples were mixed with KOH in a mass ratio of 1:1 and a certain amount of distilled water. It is worth mentioning that only the specific mass ratio was selected since we only aimed to investigate the possible impact of plasma pre-treatment on the activation

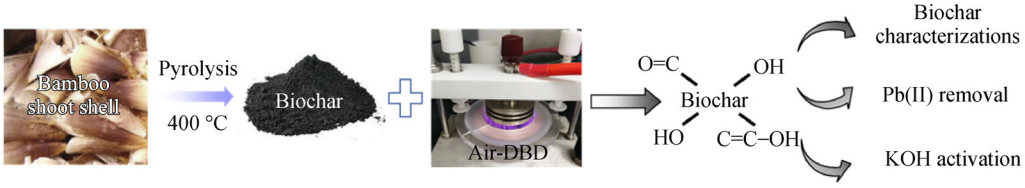

Fig. 1 The schematic diagram on the experimental procedures.

of biochar. After stirring at 60 °C until dry, the samples were heated from room temperature to 800 °C (kept for 1 h) at a heating rate of 10 °C·min^{-1} under N_2 atmosphere. After natural cooling, the activated biochar samples (termed BSSBC-AC and BSSBC-P-10-AC) were thoroughly washed with deionized water to remove any residual KOH.

2.4 Characterization

A dynamic contact angle analyzer (FTA 200) was employed to measure the water contact angles and evaluate the hydrophilicity of the biochar before and after plasma treatment at room temperature (25 °C). The thermal properties of the samples were assessed by a thermogravimetric analyzer (Netzsch STA 409 EP) in N_2 atmosphere to 800 °C (heating rate of 10 °C·min^{-1}). Fourier transform infrared spectroscopy (FTIR) spectra of the materials at the wavenumber between 500 and 4000 cm^{-1} were recorded by a FTIR spectrometer (Thermo Fisher Scientific Nicolet IS10). Raman spectra were obtained with a 532 nm laser. X-ray photoelectron spectroscopy (XPS) data were collected in a Kratos AXIS Supra photoelectron spectrometer, equipped with an Al (Kα = 1486.6 eV). The surface morphologies were investigated by scanning electron microscope (JEOL 7001F). The specific surface area and pore size distribution were determined from N_2 adsorption-desorption isotherms at 77 K in an absorptiometer (Micromeritics 3Flex). The specific surface areas were obtained by Brumauer-Emmett-Teller (BET) method and the total pore volume was derived from N_2 adsorbed at P/P_0= 0.95. Micropore volume and surface area were calculated by the t-plot method, and the pore size distribution was obtained using the non-local density functional theory.

2.5 Applications

Batch sorption experiments were conducted to compare the kinetics and isotherms of Pb^{2+} removal on the original and plasma-treated BSSBC. For each experiment, 0.1 g of the biochar was added into 50 mL Pb^{2+} aqueous solution ($Pb(NO_3)_2$) in a 100 mL Erlenmeyer flask. The mixture was placed in a mechanical shaker (120 r·min^{-1}) at room temperature for being contacted for a different duration. To test the kinetics of lead on the adsorbents at different reaction times, 100 mg·L^{-1} of Pb^{2+} solutions were used, and samples were taken at different time intervals for Pb^{2+} quantification by an inductively coupled plasma optical emission spectroscopy (ICP-OES, Perkin Elmer 8300DV). To study the adsorption isotherms, solutions with different Pb^{2+} initial concentrations (10, 20, 50, 100, 200, 250 and 300 mg·L^{-1}) were mixed with 0.1 g of biochar and shaken for 12 h. At the end of each experiment, the mixtures were immediately filtered before further quantifications were taken. The removal rate R (%) and equilibrium adsorption capacity q_e (mg·g^{-1}) were obtained by Eqs. (2) and (3) as follows:

$$R = \frac{C_0 - C_e}{C_0} \times 100\%, \quad (1)$$

$$q_e = \frac{V(C_0 - C_e)}{m}. \quad (2)$$

where C_0 and C_e refer to the initial and equilibrium Pb^{2+} concentrations (mg·L^{-1}) in solution, respectively. V is the volume of solution added (L), and m is the mass of biochar (g).

The electrodes for supercapacitors were prepared by uniformly mixing 80 wt-% of the thus-obtained activated carbons (BSSBC-AC and BSSBC-P-10-AC), 10 wt-% of polytetrafluoroethylene, and 10 wt-% of carbon black. The above mixtures (~5 mg) were coated onto nickel-foams (1 cm × 1 cm) and oven-dried (80 °C, 12 h). The electrochemical properties of the as-synthesized carbon material were firstly evaluated through the fabrication of electrode cells. The electrochemical performance was evaluated in 1 mol·L^{-1} Na_2SO_4 aqueous electrolyte with a three-electrode cell.

3 Results and discussion

3.1 Plasma-induced changes on biochar surface and structure

The operating condition of plasma treatment (30 kV of peak-peak output voltage and 9 kHz) in this work provided typical non-thermal plasma characteristics. The electrons with high temperatures sustain the discharge and enable the generation of a great number of reactive oxygen and nitrogen species. Ambient gas temperature conditions enable to avoids considerable thermal weight loss of the sample. Only a negligible sample was stuck in quartz glass and lost during all processing durations in this study. Therefore, no further considerations were taken for evaluating the sample weight loss.

One of the most common and well-accepted changes in surface properties after plasma exposure is the increased hydrophilicity [20]. As shown in Fig. S1 (cf. Electronic Supplementary Material, ESM), a very limited air plasma dose could introduce a significant decrease in the measured water contact angle, altering the BSSBC from hydrophobicity to hydrophilicity. With the water contact time of 5 s, the contact angle of BSSBC was reduced from the initial measurement value over 120° to 35.44°, 17.09°, 7.93° and 5.07° after being air-DBD treated for 1, 3, 5 and 10 min, respectively. A significantly improved hydrophilic property of BSSBC was obtained with a longer processing time. It was difficult to identify the water layer from the capture images and estimate the water contact angle for the

samples treated for longer than 10 min due to the enhanced hydrophilicity. In air discharge, many different types of highly reactive species can be generated. These species such as OH, O_3 and NO_x quickly oxidize and change the surface properties of the treated objects. Thus, surfaces with oxygen and nitrogen-containing functional groups can be easily obtained and resulted in the enhanced hydrophilicity.

As shown in Table 1, where the elemental compositions of pristine and plasma-treated BSSBC samples are listed, the mass content of carbon decreased considerably over the plasma treatment time. Specifically, compared with BSSBC, a decrease of 1.45%, 3.87% and 6.71% in carbon content was observed for BSSBS-P-5, BSSBC-P-10 and BSSBA-P-20, respectively. It is considered that abundant chemically and physically reactive species containing O and N within the plasma induce substantially enhanced surface reactions with the carbon, leading to the generation of surface functional groups and the reduced relative carbon contents on the biochar [11,12]. While the case for the change of oxygen content was opposite, with the value of oxygen content increased from 27.46% to 29.20%, 30.96% and 33.90% corresponding to 5, 10 and 20 min of plasma exposure. To further confirm the changes (or introduction) of functional groups and chemical composition, FTIR and XPS measurements were conducted with results illustrated in Fig. 2. As Fig. 2(a) shows, after plasma treatment, a significant band increase was observed at around 1710 cm^{-1}, which is the characteristic band of C = O (carbonyl, ester, carboxylic, etc.) stretching vibrations [21], indicating the successful introduction of extra oxygen functional groups and the oxidation of biochar. The absorption peak at ~1380 cm^{-1} also increased significantly. There are mainly two reasons for changes in this range. One is the in-plane bending vibration peak of –CH, while the other is in-plane bending vibration peak of –OH belonging to primary alcohols [21,22]. Considering that there are many –CH bonds in the BSSBC itself, certain changes in them may not lead to a vital peak fluctuation; thus, we assumed that the reason should be more likely due to the increase of –OH. Also, the C–N stretching vibration band (~875 cm^{-1}) [21] increased after plasma treatment, revealing the introduction of nitrogen-containing groups.

XPS reveals the changes in chemical composition and surface functionality of BSSBC before and after plasma treatment. The high-resolution C1s spectra of the samples are shown in Figs. 2(b–d), with the optimum fitting result achieved by deconvolution of four peaks for each C1s spectrum. Table 2 listed the electron binding energy (eV) and relative intensity of each peak for the relative chemical bonds [11,21]. The peak for C–C/C = C was the most primary one for each sample, taking up to ~72% for the pristine biochar and considerably reducing to 63% and 58.21% after being plasma treated for 5 and 10 min, respectively. It can also be seen from the table that the contents of oxygen-containing bonds experienced substantial increases after plasma treatment. Particularly, carbonyl group (C = O) content almost doubled with a plasma exposure (increasing from 7.25% for original BSSBC to 13.24% and 14.00% for BSSBC-P-5 and BSSBC-P-5, respectively), and the value for C–O also increased substantially from 12.57% to over 18%. These results were consistent with the changing tendency of element contents from the element analyzer and the FTIR outcomes.

To further evaluate and understand plasma effects on the physicochemical properties of biochar, further surface characterizations were performed. SEM images of BSS before and after pyrolysis and plasma-treated BSSBC samples are shown in Fig. S2 (cf. ESM). After pyrolysis, the relatively periodic and regular structure of lignocellulose and smooth surface morphology was altered. With the plasma exposure, the surface roughness enhanced over the treatment duration, while the particle size reduced (especially, particles with much more homogeneous and smaller size distribution were observed for the BSSBC-P-10), consistent with results in the literature [10]. Other important characterizations are presented in Fig. 3. Figure 3(a) shows the Raman spectra of untreated and plasma-treated biochar. The characteristic peak at 1530–1610 cm^{-1} (G-band) corresponds to individual graphite dominated by sp^2 bonds, while that around 1320–1370 cm^{-1} (D-band) indicates a disordered and irregular structure [10,21]. It can be found from the figure that no significant changes in the Raman features were introduced by plasma. Only the ratio of I_D/I_G decreased slightly from 0.90 to 0.83 after plasma treatment for 20 min, indicating a lower proportion of sp^3 carbons or the presence of a higher proportion of graphitic

Table 1 Properties of the pristine and plasma-treated BSSBC concluded from different characterizations

Samples	Element content/wt-%				TGA			BET	
	C	H	N	O [a)]	15% loss T/°C	Maximum loss T/°C	Total loss/wt-%	$S^{b)}$/($m^2 \cdot g^{-1}$)	$V^{c)}$/($cm^3 \cdot g^{-1}$)
BSSBC	65.62	4.50	2.42	27.46	427.1	441.2	32.0	2.4	0.0065
BSSBC-P-1	65.45	4.38	2.44	27.73	413.6	440.1	33.3	–	–
BSSBC-P-5	64.17	4.15	2.68	29.20	390.4	300.8; 437.1	34.5	6.2	0.0116
BSSBC-P-10	61.75	4.20	3.09	30.96	345.4	301.3; 439.1	37.8	9.2	0.0137
BSSBC-P-20	58.91	3.88	3.21	33.90	284.0	301.5; 438.0	43.6	14.4	0.0186

a) O content was estimated according to the assumption that all samples only contain C, H, N and O; b) surface area was calculated using BET method around P/P_0 = 0.05–0.3 with a correlation coefficient more than 0.9999; c) total pore volume (⩽100 nm) was determined using the NFDFT method.

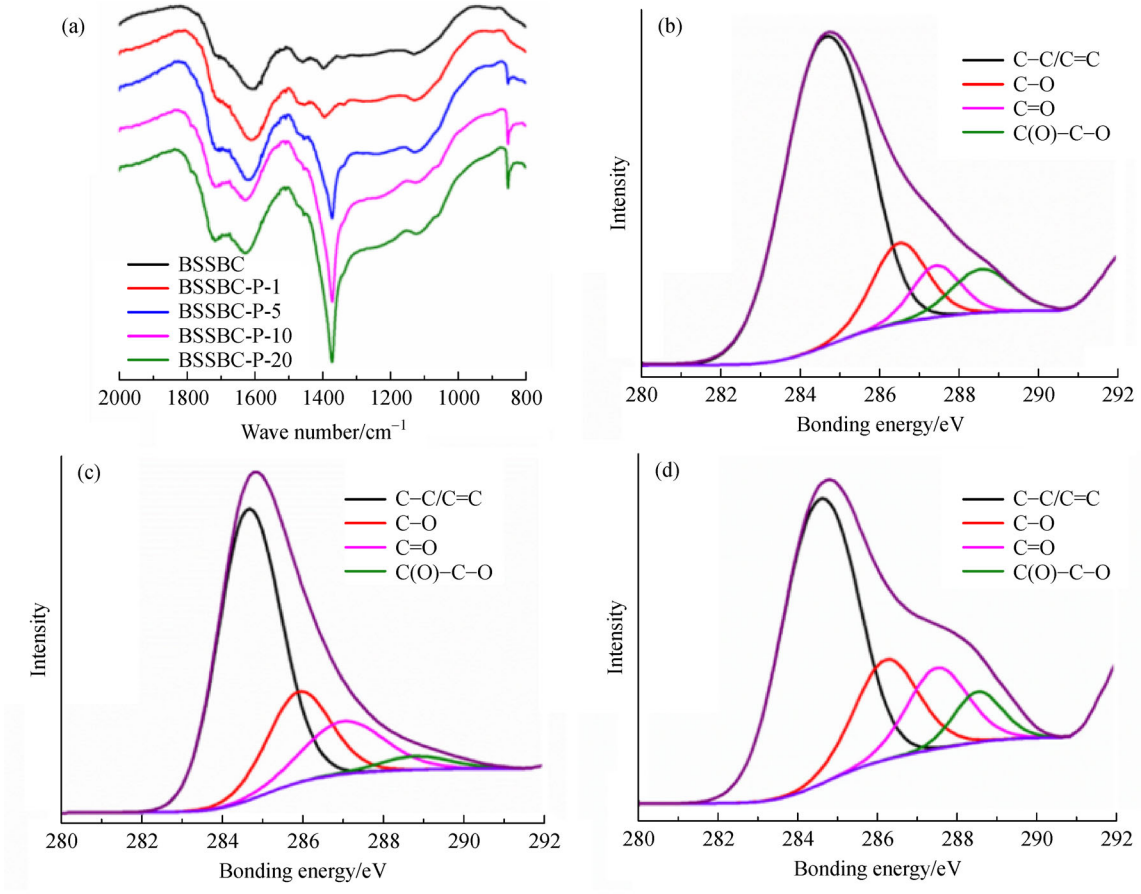

Fig. 2 (a) FTIR spectra of the pristine and plasma-treated BSSBC and XPS spectra of C1s of (b) BSSBC, (c) BSSBC-P-5 and (d) BSSBC-P-10.

Table 2 Chemical bonds of the pristine and plasma-treated BSSBC from XPS C1s

Bonds	Electron binding energy/eV	Relative intensity/%		
		BSSBC	BSSBC-P-5	BSSBC-P-10
C–C/C = C	284.5	71.95	63.50	59.21
C–O	285.8	12.57	18.23	19.21
C = O	287.1	7.25	13.24	14.00
C(O)–O–C	288.7	7.50	4.24	6.97

structure [10,18,21]. The thermogravimetric properties of these samples were illustrated in Fig. 3(b) and concluded in Table 1. Similar TGA curves were obtained, with the maximum weight loss at around 440 °C for all biochar samples, indicating that the intrinsic characteristics and compositions of the biochar were not significantly modified. However, some changes can also be observed over the treatment durations. For example, the characteristic temperature for 15% weight loss (T) showed a negative linear correlation ($T = -7.1064 \times t + 423.27$, $R^2 = 0.994$) with the plasma treatment time (t, min), while a positive linear correlation ($m = 0.5666 \times t + 32.16$, $R^2 = 0.993$) was confirmed for the total weight loss (m) over the time. As expected and illustrated in Fig. 3(c) and Table 1, there was not obvious porous structure in the biochar samples due to the low temperature (400 °C) being used for pyrolysis. Yet, the surface area (S) of the BSSBC-P increased over exposure time, and again a positive linear correlation was found ($S = 0.5909 \times t + 2.88$, $R^2 = 0.992$).

3.2 Plasma-enhanced adsorption capacity of biochar towards metal ions

With the fast development of modern industry, wastewater containing heavy metal ions (such as Pb^{2+}, Cu^{2+}, Ni^{2+} and Cr^{3+}) and organic pollutants with potential toxicity and carcinogenic effects has been causing a series of environ-

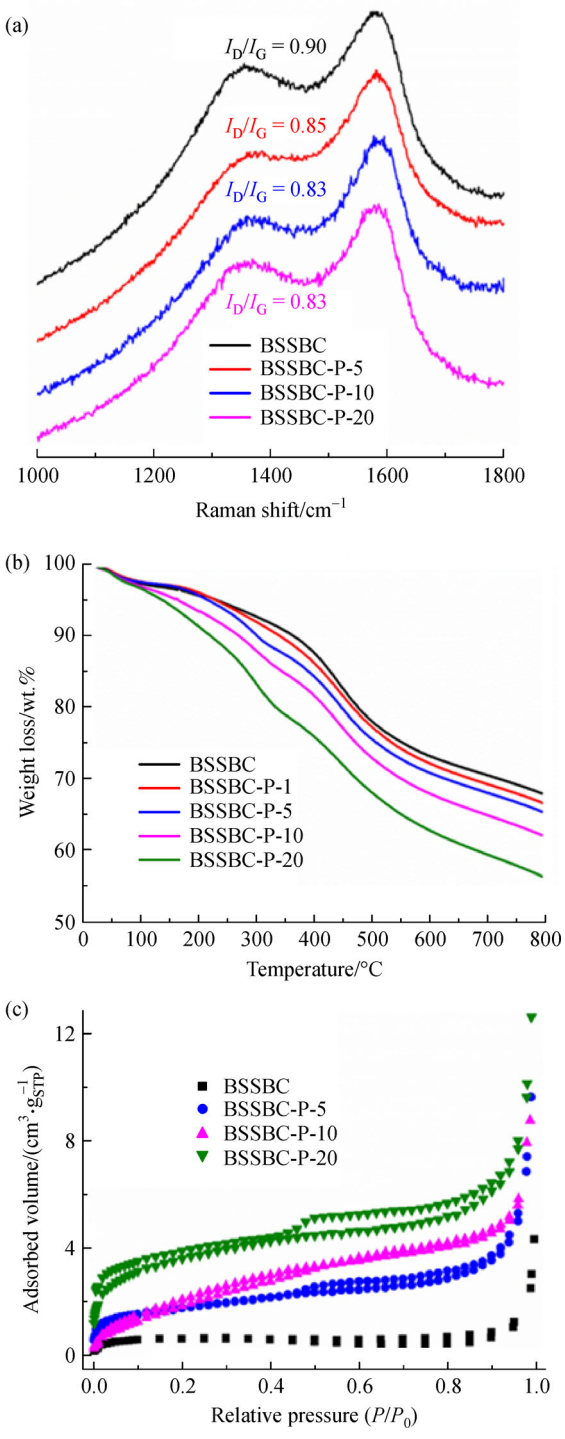

Fig. 3 (a) Raman, (b) TGA and (c) N_2 adsorption/desorption isotherms of the pristine and plasma-treated BSSBC.

mental and health problems. Adsorption by low-cost biomass-derived products, especially the biochar and activated carbon, is a highly effective, widely applicable, and easy-to-operate method suitable for different kinds of wastewater purification [22,23]. However, the adsorption efficiencies and capacities of such crude biochar are generally far from satisfactory; thus, further modification or functionalization is usually required. Here, to verify whether the air plasma treatment was able to enhance the performances of BSSBC being used as a bio-adsorbent, Pb^{2+} was used as a model metal pollutant due to its common use and high toxicity with the adsorption results illustrated in Fig. 4.

Clearly, the Pb^{2+} removal rates were significantly enhanced in the groups with plasma treatment. The time for adsorption equilibrium for BSSBS was > 12 h, while BSSBC-P-10 and BSSBC-P-20 reduced to 8 and 4 h, respectively (Fig. 4(a)). Plasma treatment was able to enhance the adsorption efficacy. For example, in the first hour, only less than 26% of Pb^{2+} was removed by the original BSSBC, but the removal was 2.8-time higher increased as 70.45% with BSSBC-P-10. The corresponding equilibrium removal (at 12 h) for these biochars was found to be ~72.42% (BSSBC), 90.01% (BSSBC-P-10) and 64.11% (BSSBC-P-20). The enhancement of pollutant removal rate and capacity after plasma treatment can be attributed to the enrichment of surface functional groups and the changes of physical properties, which enhanced the contact of Pb^{2+} ions with the biochar and increased the active adsorption sites. Although it seems that a longer plasma exposure duration (20 min) would shorten the time required for adsorption equilibrium due to the further increase of hydrophilicity. Yet, an unsatisfactory final adsorption capacity, lower than that of the untreated BSSBS, was observed. This might be due to the excessive hydrophilicity which causes a higher affinity of water on the adsorbent surface than the targeted adsorbate Pb^{2+}. The water molecules may consume part of the active sites and prevent the efficient adsorption of Pb^{2+}, hence negatively affect the removal of Pb^{2+}.

To better assess the adsorption capacity of these biochar adsorbents, Pb^{2+} adsorption isotherm studies were conducted, and the results were fitted by the commonly used Langmuir isothermal adsorption model (results in Fig. 4(b) and Table S1 (cf. ESM)) [24,25]. The Langmuir model considers that the monolayer adsorption occurs on the uniform surface of the adsorbent. The equation is expressed as follows:

$$\frac{1}{q_e} = \frac{1}{Q \times b} \times \frac{1}{C_e} + \frac{1}{Q}, \tag{3}$$

where C_e is equilibrium adsorption concentration (mg·L^{-1}), and q_e corresponds to the equilibrium adsorption capacity (mg·g^{-1}). Q (mg·g^{-1}) represents the maximum adsorption capacity, and b (L·mg^{-1}) is the Langmuir constant. Results revealed that at the same condition of water contact for 12-h duration, the Pb^{2+} removal capacity of all investigated initial concentrations was consistently in the order of BSSBC-P-10 > BSSBC > BSSBC-P-20, consistent with the results from Fig. 4(a). The results were well fitted by the Langmuir model with all $R^2 > 0.99$, indicating

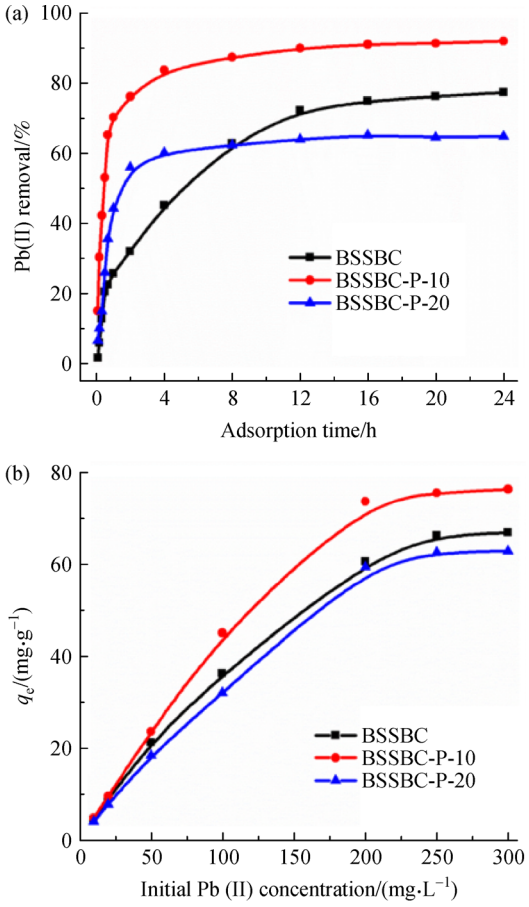

Fig. 4 (a) Pb^{2+} removal kinetics and (b) adsorption isotherms using the pristine or plasma-treated BSSBC as the adsorbent.

that the monolayer adsorption dominated at this investigating temperature. Based on the fitting results, the maximum Pb^{2+} adsorption capacity of BSSBC-P-10 was calculated to be 94.34 mg·g^{-1}, increased by 41.50% when compared to the original BSSBS (66.67 mg·g^{-1}).

3.3 Biochar activation and activated biochar for energy storage application

Developed porous structures with optimized size distribution of pores are usually the prerequisites for biochar-based materials to be utilized for energy storage and catalytic applications [1,26]. Here, activation of the BSSBC was conducted using a widely-used KOH-based method. It needs to be noted that a specific heating procedure was chosen with only a low mass ration of biochar and KOH (1:1), since the main aim of this investigation was to understand whether the plasma pre-treatment could somehow lower the dosage of the chemical activator (here KOH) and/or assist the following activation. The most important properties (specific surface area, pore volume and pore size distribution) of the activated biochars (BSSBS-AC and BSSBC-P-10-AC) were obtained from N_2 adsorption/desorption isotherms illustrated in Fig. 5 and Table 3. The BET surface area of the KOH-activated BSSBC (BSSBC-AC) was determined to be 1094.57 m^2·g^{-1}, consisting of a micropore surface area of 862.07 m^2·g^{-1}. With plasma pre-treatment before activation, the BSSBC-P-10-AC was found to be developed a higher BET surface area of 1336.71 m^2·g^{-1} and micropore surface area of 1086.17 m^2·g^{-1}. The pore volume of the BSSBC-P-AC was also enhanced. Specifically, the total pore volume was increased from 0.5376 to 0.6584 cm^3·g^{-1}, and an increase of 23.93% and 19.65% was observed towards the micropore and mesopore volume, respectively. When the amount of the chemical activator (KOH) used was the same and insufficient, the increase in the surface area and pore volume in the plasma pre-treatment group suggested that KOH was better utilized during the activation. This can be associated with surface oxidation and functionalization, which also enhanced the KOH affinity of biochar after plasma treatment [27,28].

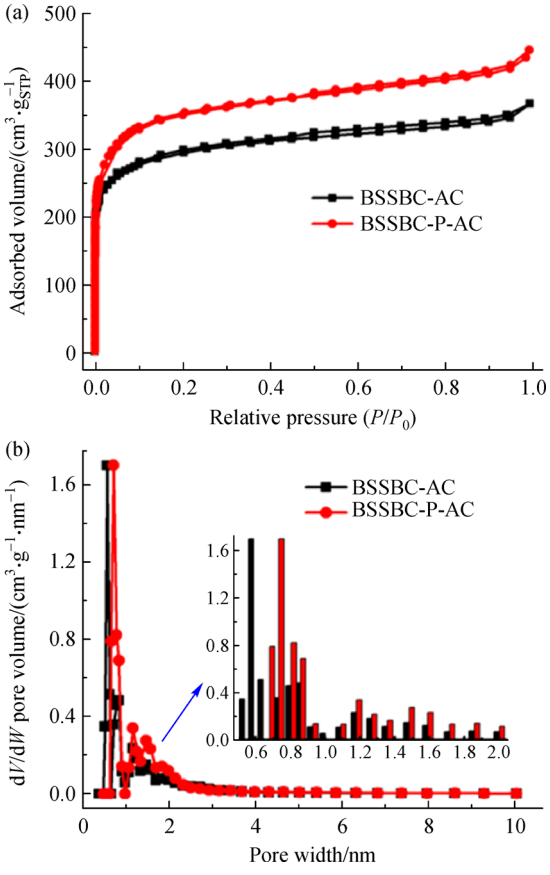

Fig. 5 (a) N_2 adsorption/desorption isotherms and (b) pore size distribution curves of the BSSBC-AC and BSSBC-P-10-AC.

Additionally, the activated biochars were applied as supercapacitor electrodes to evaluate and compare their performances in energy storage applications. Cyclic voltammetry (CV) and galvanostatic charge/discharge

Table 3 Surface areas and pore volumes BCCBC-AC and BSSBC-P-10-AC

Sample	BET surface area/ ($m^2 \cdot g^{-1}$)	Micropore surface area/ ($m^2 \cdot g^{-1}$)	Pore volume/ ($cm^3 \cdot g^{-1}$)	Micropore volume/ ($cm^3 \cdot g^{-1}$)	Mesopore volume/ ($cm^3 \cdot g^{-1}$)
BSSBC-AC	1094.57	862.07	0.5376	0.3539	0.1837
BSSBC-P-10-AC	1336.71	1086.17	0.6584	0.4386	0.2198

(GCD) measurements shown in Fig. 6 were performed using 6 mol·L^{-1} KOH electrolyte. The CV curves of both BSSBC-AC and BSSBC-P-10-AC showed typical square shapes during the investigating potentials (–1 to 0 V), indicating the ideal double-layer capacitive behavior [26]. As illustrated in Fig. 6(b), the GCD plots of BSSBC-AC and BSSBC-P-10-AC had isosceles triangle shapes at a current density of 0.5 A·g^{-1}, implying good charge and discharge reversibility. From the GCD curves, corresponding specific capacitances for both activated biochar samples could be calculated. According to the charging curves, the specific capacitance of the BSSBC-P-10-AC was 175.5 F·g^{-1}, which was more than 30% higher than that of the BSSBC-AC (134.7 F·g^{-1}). It is consistent with the measured physical properties, further confirming the potentials of plasma pre-treatment in preparing better-performance biochar-based functional materials.

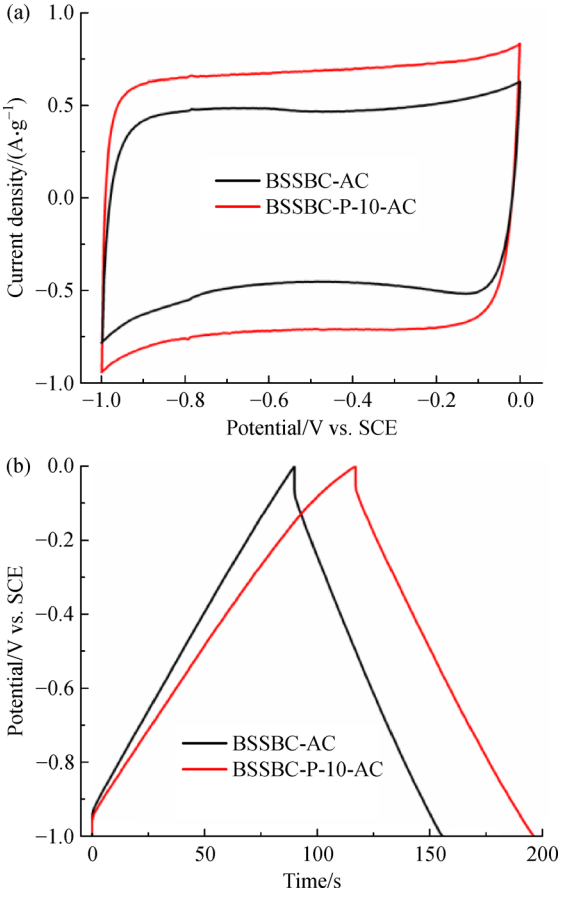

Fig. 6 Electrochemical performances of the BSSBC-AC and BSSBC-P-10-AC: (a) CV diagram at the scan rate of 5 mV·s^{-1} and (b) GCD profiles at a current density of 1.5 A·g^{-1}.

4 Conclusions

In this study, an air DBD plasma pre-treatment was applied for the direct and chemical-free biochar modification. Compared with the pristine BSSBC, the plasma treated BSSBC-P-10 showed an increased oxygen content by more than 10% mainly due to the enhanced contents of C = O and C–O functional groups on the biochar surface. When used as an adsorbent for metal ion removal, the BSSBC-P-10 was observed with a much-enhanced Pb^{2+} removal rate and maximum removal capacity (94.34 mg·g^{-1}). The activated carbon derived from the BSSBC-P-10 showed a developed surface area and pore structure, which resulted in an enhanced capacitance. This study demonstrates that the non-thermal plasma processing can effectively enhance the surface functionality of biochar and also assist the reduction of chemicals usage in the activation process.

Acknowledgements This work was supported by the National Natural Science Foundation of China (Grant No. 52007023), the Natural Science Foundation of Liaoning Province, China (Grant Nos. 2020-BS-073, 2019-ZD-0160), the China Postdoctoral Science Foundation (Grant No. 2019M661107), the Dalian Maritime University basic scientific research business expenses key scientific research cultivation project (Grant No. 3132020371) and the Fundamental Research Funds for the Central Universities (Grant No. 3132021159). Rusen Zhou thanks the financial support from QUT Postgraduate Research Award and Faculty Write Up Scholarship. Kostya (Ken) Ostrikov thanks the Australian Research Council (ARC) and QUT Centre for Materials Science for partial support.

Electronic Supplementary Material Supplementary material is available in the online version of this article at https://dx.doi.org/10.1007/s11705-021-2070-x and is accessible for authorized users.

References

1. Liu W, Jiang H, Yu H. Development of biochar-based functional materials: toward a sustainable platform carbon material. Chemical Reviews, 2015, 115(22): 12251–12285
2. Mohanty A K, Vivekanandhan S, Pin J M, Misra M. Composites from renewable and sustainable resources: challenges and innovations. Science, 2018, 362(6414): 536–542
3. Fu C, Li Z, Sun Z, Xie S. A review of salting-out effect and sugaring-out effect: driving forces for novel liquid-liquid extraction of biofuels and biochemicals. Frontiers of Chemical Science and

Engineering, 2020, doi: 10.1007/s11705-020-1980-3
4. Zhou R, Zhou R, Wang S, Mihiri Ekanayake U G, Fang Z, Cullen P J, Bazaka K, Ostrikov K K. Power-to-chemicals: low-temperature plasma for lignin depolymerisation in ethanol. Bioresource Technology, 2020, 318: 123917
5. Xue Y, Gao B, Yao Y, Inyang M, Zhang M, Zimmerman A R, Ro K S. Hydrogen peroxide modification enhances the ability of biochar (hydrochar) produced from hydrothermal carbonization of peanut hull to remove aqueous heavy metals: batch and column tests. Chemical Engineering Journal, 2012, 200-202: 673–680
6. Yang G X, Jiang H. Amino modification of biochar for enhanced adsorption of copper ions from synthetic wastewater. Water Research, 2014, 48: 396–405
7. Zhong Y, Zhang P, Zhu X, Li H, Deng Q, Wang J, Zeng Z, Zou J J, Deng S. Highly efficient alkylation using hydrophobic sulfonic acid-functionalized biochar as a catalyst for synthesis of high-density biofuels. ACS Sustainable Chemistry & Engineering, 2019, 7(17): 14973–14981
8. Sizmur T, Fresno T, Akgül G, Frost H, Moreno-Jiménez E. Biochar modification to enhance sorption of inorganics from water. Bioresource Technology, 2017, 246: 34–47
9. Gupta R K, Dubey M, Kharel P, Gu Z, Fan Q H. Biochar activated by oxygen plasma for supercapacitors. Journal of Power Sources, 2015, 274: 1300–1305
10. Zhou R, Zhou R, Zhang X, Bazaka K, Ostrikov K K. Continuous flow removal of acid fuchsine by dielectric barrier discharge plasma water bed enhanced by activated carbon adsorption. Frontiers of Chemical Science and Engineering, 2019, 13(2): 340–349
11. Neyts E C. Special Issue on future directions in plasma nanoscience. Frontiers of Chemical Science and Engineering, 2019, 13(2): 199–200
12. Wang X, Zhou R, Zhang C, Xi S, Jones M W M, Tesfamichael T, Du A, Gui K, Ostrikov K K, Wang H. Plasma-induced on-surface sulfur vacancies in $NiCo_2S_4$ enhance the energy storage performance of supercapatteries. Journal of Materials Chemistry. A, Materials for Energy and Sustainability, 2020, 8(18): 9278–9291
13. Zhou R, Zhou R, Xian Y, Fang Z, Lu X, Bazaka K, Bogaerts A, Ostrikov K K. Plasma-enabled catalyst-free conversion of ethanol to hydrogen gas and carbon dots near room temperature. Chemical Engineering Journal, 2020, 382: 112745
14. Xin Y, Sun B, Zhu X, Yan Z, Zhao X, Sun X. Hydrogen production from ethanol decomposition by pulsed discharge with needle-net configurations. Applied Energy, 2017, 206: 126–133
15. Xin Y, Sun B, Zhu X, Yan Z, Zhao X, Sun X. Carbon nanoparticles production by pulsed discharge in liquid alcohols. Vacuum, 2018, 151: 90–95
16. Bogaerts A, Neyts E C. Plasma technology: an emerging technology for energy storage. ACS Energy Letters, 2018, 3(4): 1013–1027
17. Zhao T, Ullah N, Hui Y, Li Z. Review of plasma-assisted reactions and potential applications for modification of metal-organic frameworks. Frontiers of Chemical Science and Engineering, 2019, 13(3): 444–457
18. Zhou R, Zhou R, Alam D, Zhang T, Li W, Xia Y, Mai-Prochnow A, An H, Lovell E C, Masood H, Amal R, Ostrikov K K, Cullen P J. Plasmacatalytic bubbles using CeO_2 for organic pollutant degradation. Chemical Engineering Journal, 2021, 403: 126413
19. Ye L, Zhang J, Zhao J, Luo Z, Tu S, Yin Y. Properties of biochar obtained from pyrolysis of bamboo shoot shell. Journal of Analytical and Applied Pyrolysis, 2015, 114: 172–178
20. Kazak O, Eker Y R, Bingol H, Tor A. Novel preparation of activated carbon by cold oxygen plasma treatment combined with pyrolysis. Chemical Engineering Journal, 2017, 325: 564–575
21. Siow K S, Kumar S, Griesser H J. Low-pressure plasma methods for generating non-reactive hydrophilic and hydrogel-like bio-interface coatings—a review. Plasma Processes and Polymers, 2015, 12(1): 8–24
22. Zhang B, Xu P, Qiu Y, Yu Q, Ma J, Wu H, Luo G, Xu M, Yao H. Increasing oxygen functional groups of activated carbon with non-thermal plasma to enhance mercury removal efficiency for flue gases. Chemical Engineering Journal, 2015, 263: 1–8
23. Peng B, Zhou R, Chen Y, Tu S, Yin Y, Ye L. Immobilization of nano-zero-valent irons by carboxylated cellulose nanocrystals for wastewater remediation. Frontiers of Chemical Science and Engineering, 2020, 14(6): 1006–1072
24. Ouni L, Ramazani A, Fardood S T. An overview of carbon nanotubes role in heavy metals removal from wastewater. Frontiers of Chemical Science and Engineering, 2019, 13(2): 1–22
25. Wang F, Pan Y, Cai P, Guo T, Xiao H. Single and binary adsorption of heavy metal ions from aqueous solutions using sugarcane cellulose-based adsorbent. Bioresource Technology, 2017, 241: 482–490
26. Thubsuang U, Chotirut S, Thongnok A, Promraksa A, Nisoa M, Manmuanpom N, Wongkasemjit S, Chaisuwan T. Facile preparation of polybenzoxazine-based carbon microspheres with nitrogen functionalities: effects of mixed solvents on pore structure and supercapacitive performance. Frontiers of Chemical Science and Engineering, 2020, 14(6): 1072–1086
27. Zhou R, Zhou R, Zhang X, Fang Z, Wang X, Speight R, Wang H, Doherty W, Cullen P J, Ostrikov K K, Bazaka K. High-performance plasma-enabled biorefining of microalgae to value-added products. ChemSusChem, 2019, 12(22): 4976–4985
28. Jain A, Xu C, Jayaraman S, Balasubramanian R, Lee J Y, Srinivasan M P. Mesoporous activated carbons with enhanced porosity by optimal hydrothermal pre-treatment of biomass for supercapacitor applications. Microporous and Mesoporous Materials, 2015, 218: 55–61